Report Title: “Substituted iron oxides” for the grant entitled “Laser processing of advanced magnetic materials”

Type of Report: Semi-Annual

Reporting Period Start Date: September 12, 2003

Reporting Period End Date: March 11, 2004

Principal Author: Professor Monica Sorescu

Date Report was Issued: March 1, 2004

DOE Award Number: DE-FC26-02NT41595

Name and Address of Submitting Organization: Duquesne University, Bayer School of Natural and Environmental Sciences, Department of Physics, Pittsburgh, PA 15282-0321

DISCLAIMER

This report was prepared as an account of work sponsored by an agency of the United States Government. Neither the United States Government nor an agency thereof, nor any of their employees, makes any warranty, express or implied, or assumes any legal liability or responsibility for the accuracy, completeness, or usefulness of any information, apparatus, product, or process disclosed, or represents that its use would not infringe privately owned rights. Reference herein to any specific commercial product, process, or service by trade name, trademark, manufacturer, or otherwise does not necessarily constitute or imply its endorsement, recommendation, or favoring by the United States Government or any agency thereof. The views and opinions of authors expressed herein do not necessarily reflect those of the United States Government or any agency thereof.

ABSTRACT

Structural and morphological characteristics of (1-x)α-Fe_2O_3-xSnO_2 (x=0.0-1.0) nanoparticles obtained under hydrothermal conditions have been investigated by X-ray diffraction (XRD), transmission Mössbauer spectroscopy, scanning (SEM) and transmission electron microscopy (TEM) as well as energy dispersive X-ray analysis (EDX). On the basis of the Rietveld structure refinements of the XRD spectra at low tin concentrations, it was found that Sn^{4+} ions partially substitute for Fe^{3+} at the octahedral sites and also occupy the interstitial octahedral sites which are vacant in α-Fe_2O_3 corundum structure. A phase separation of α-Fe_2O_3 and SnO_2 was observed for $x \geq 0.4$: the α-Fe_2O_3 structure containing tin decreases simultaneously with the increase of the SnO_2 phase containing substitutional iron ions. The mean particle dimension decreases from 70 nm to 6 nm, as the molar fraction x increases up to x=1.0. The estimated solubility limits in the nanoparticle system (1-x)α-Fe_2O_3-xSnO_2 synthesized under hydrothermal conditions are: $x \leq 0.2$ for Sn^{4+} in α-Fe_2O_3 and $x \geq 0.7$ for Fe^{3+} in SnO_2. These findings are in press in the Journal of Physics and Chemistry of Solids.

TABLE OF CONTENTS

LIST OF GRAPHICAL MATERIAL

Figure 7. The lattice parameters of the SnO_2 phase in (1-x)α-Fe_2O_3-xSnO_2 samples versus iron molar concentration (1-x); (a) the lattice parameter *a* and (b) the lattice parameter *c*. The lines are guides to the eye.

Figure 8. ^{57}Fe Mössbauer spectra of (1-x)α-Fe_2O_3-xSnO_2 samples at different molar concentration x; (a) x=0.0, (b) x=0.08, (c) x=0.21, (d) x=0.40, (e) x=0.70, and (f) x=0.86.

Figure 9. Representative Mössbauer spectra (a, b, c) of the nanoparticle system (1-x)α-Fe_2O_3-xSnO_2 fitted with hyperfine magnetic field distribution together with the calculated magnetic hyperfine field distribution probabilities (A, B, C); (a) x=0.08, (b) x=0.21, (c) x=0.31.

Figure 10. Relative Mössbauer areas of magnetic and paramagnetic phases versus molar concentration x, for (1-x)α-Fe_2O_3-xSnO_2 samples (x=0.0 ÷0.9).

Figure 11. Scanning electron microscopy examination of (1-x)α-Fe_2O_3-xSnO_2 system for x=0.4.

Figure 12. Energy dispersive energy analysis of (1-x)α-Fe_2O_3-xSnO_2 system for x=0.4.

INTRODUCTION

During the last few years much attention has been paid to the synthesis and study of semiconducting oxides due to their sensing properties in the detection of toxic or dangerous gases (such as CO, NO_2, Cl_2, CH_4) [1-3]. Enhanced gas sensing properties are expected for nanostructured semiconducting oxides due to the great surface activity provided by their high surface areas. Being a promising gas sensing material, the oxide system (1-x)α-Fe_2O_3-xSnO_2 has been prepared by various methods at nanometric scale [4-8], especially at low tin content. The solubility of SnO_2 in α-Fe_2O_3 is less than 1 mol % below 1073 K, while it increases to 4 mol % at 1473 K [9,10]. High energy ball milling was used to extend the range of composition at about 6 mol % [4]. It was suggested that the content of Sn^{4+} may have an important role in the gas sensing activity of this compound. However, the mechanism of sensing in (1-x)α-Fe_2O_3-xSnO_2 is not well understood due to an incomplete understanding of its microstructure characteristics.

The structure of α-Fe_2O_3 (hematite) is based on hexagonal close packing of oxygen with iron in 2/3 of the octahedral vacancies. The lattice parameters are: a = 5.038 Å, c = 13.772 Å. The space group is (S.G. 167) R32/c. At low temperature it is antiferromagnetic with spins oriented along the electric field gradient axis. When the temperature is raised, to about 260 K a spin flop transition (known as the Morin transition) occurs and the spins shift by about 90° becoming canted to each other. This transition results in a weak ferromagnetic moment along the electric field gradient axis. SnO_2 is known to crystallize in tetragonal, orthorhombic or cubic structures. The most common structure is the tetragonal phase (rutile type structure) known as cassiterite, with a = 4.7382(4) Å, c = 3.1871(1) Å and the space group (S. G. 136) P42/mnm.

In the early stage of research on this material it was believed that Sn^{4+} enters substitutionally in the hematite lattice with the subsequent formation of cationic and anionic

vacancies. Later, it was shown by X-ray diffraction (XRD) spectra refinements [11] that the tin ions occupy two distinct sites. In addition to partly substituting for Fe^{3+} in octahedral sites they also occupy vacant interstitial octahedrals in the hematite structure. Besides XRD and EXAFS, transmission Mössbauer spectroscopy investigations on both ^{57}Fe and ^{119}Sn isotopes have been performed for a better understanding of the site occupancy of Sn^{4+} in the hematite lattice [12]. Finally, it was found that the degree of order given by the mentioned approach is far from perfect and that the microstructural defects are highly sensitive to tin content and preparative methods.

In this paper we report the synthesis of the $(1-x)\alpha-Fe_2O_3-xSnO_2$ nanoparticles via a hydrothermal route over the entire concentration range of x=0.0 to x=1.0. X-ray (XRD) and electron diffraction including selected area electron diffraction (SAED), transmission Mössbauer spectroscopy, transmission and scanning electron microscopy as well as energy dispersive X-ray analysis (EDX) have been used to correlate the structure, morphology and phase dynamics in this system, in correlation with the tin concentration. Experimental evidence of the solubility limits of Sn^{4+} in the hematite structure and of Fe^{3+} in SnO_2 are discussed.

EXECUTIVE SUMMARY

This work proposes and achieves the hydrothermal synthesis of (1-x)α-Fe_2O_3-xSnO_2 (x=0.0-1.0) nanoparticles. The system has been investigated by X-ray diffraction (XRD), transmission Mössbauer spectroscopy, scanning (SEM) and transmission electron microscopy (TEM) as well as energy dispersive X-ray analysis (EDX). Based on the Rietveld structure refinements of the XRD spectra at low tin concentrations, it was found that Sn^{4+} ions partially substitute for Fe^{3+} at the octahedral sites and also occupy the interstitial octahedral sites which are vacant in α-Fe_2O_3 corundum structure. For $x \geq 0.4$, a phase separation of α-Fe_2O_3 and SnO_2 was observed: the α-Fe_2O_3 structure containing tin decreases simultaneously with the increase of the SnO_2 phase containing substitutional iron ions. As determined from TEM, the mean particle dimension decreases from 70 nm to 6 nm, as the molar fraction x increases up to x=1.0.

EXPERIMENTAL

A series of (1-x)α-Fe_2O_3-xSnO_2 (x=0.0-1.0) was prepared under hydrothermal conditions. The hydrothermal syntheses were performed in a 50 mL Teflon lined stainless steel autoclave, starting with an aqueous mixture of iron (III) chloride hexahydrate, $FeCl_3 \cdot 6H_2O$, and tin (IV) chloride pentahydrate, $SnCl_4 \cdot 5H_2O$. A 25% ammonium hydroxide solution was used as precipitation agent to attain a pH equal to 8. The suspension of precipitated solids was heated in autoclave at 200 ˚C for 4 hours and then quenched to room temperature. The corresponding vapor pressure at 200 ˚C was about 15 atm. The resulted precipitate was filtered, washed with water until no chloride ions were detected by silver nitrate solution and then dried in a furnace at 105 ˚C. The structure of the powders was examined using Rigaku D-2013 X-ray diffractometer with CuK_α radiation (λ=1.540598 Å). The ^{57}Fe Mössbauer spectra were recorded at room temperature using a ^{57}Co in Rh matrix source and an MS-1200 constant acceleration spectrometer. The sample thickness was 7 mg Fe/cm^2. JEOL 200 CX and Topcon 002B electron microscopes were used for the electron microscopy analyses. The actual level of tin molar content x was determined by EDX using a Kevex system installed on the Topcon microscope**.** The EDX analyses were carried out using a 30 nm electron beam spot. Measurements were performed on several different sites on each specimen, in order to examine the compositional uniformity. The determined average values of x, for the analyzed series of mixed samples are: x=0.08, x=0.15, x=0.21, x=0.31, x=0.40, x=0.56, x=0.70, x=0.77 and x=0.86.

RESULTS AND DISCUSSION

The X-ray diffraction patterns of the hydrothermally synthesized samples have been analyzed to study the phase structure in relation to the tin concentration x. In Figure 1 selected XRD spectra from the entire concentration range are shown. Dramatic changes in phase composition and peak broadening are observed over the range of tin content x. At x=0.0, the XRD spectrum (Figure 1a) corresponds to pure α-Fe_2O_3 (JCPDS-ICDD card No. 13-534) synthesized under hydrothermal conditions from $FeCl_3 \cdot 6H_2O$. Small changes in the line positions and broadening are observed in Figure 1b, at x=0.08. In Figure 1c (x=0.21) the characteristic lines of SnO_2 (JCPDS-ICDD card No. 41-1445) appear. As the tin content in the samples increases, the amount of α-Fe_2O_3 phase diminishes for x=0.86 (Figure 1f) and only the large peaks corresponding to SnO_2 structure are observed. At x=1.0 (Figure 1g) XRD pattern corresponds to pure, tetragonal SnO_2 phase. The observed increase in the peak broadening is due to decreasing grain size, as shown by particle dimension calculation using the Scherrer equation [13]. The plot of particle dimension versus tin content x in the system is shown in Figure 2 together with the best fit of the data - an exponential decay curve (continuous line). This behavior reveals the fast decrease of the mean particle diameter by increasing the tin content in the hydrothermal system. The particle distribution, ranging from 70 to approximately 6 nm, was confirmed by TEM investigations. Representative TEM images are shown in Figure 3. In Figure 3a the morphology of the pure hematite crystallized under hydrothermal conditions is shown. The crystallites are without defects and generally have the typical rhombohedral morphology of hematite. In this habit, the main surface crystallographic plane is (102). For x=0.08, (Figure 3b), the morphology is nearly the same, but the hematite crystallites are smaller

and some lattice defects are evident. At x = 0.15, the morphology changes and the crystallites are highly imperfect (Figure 3c). Some crystallites are as large as 100 nm, but the average crystallite, as determined by XRD, is much smaller. For these samples, EDX measurements were performed by focusing the electron beam on one or two crystallites. The results were similar with a variation of less than 2 %, reflecting a rather uniform composition in the sample. Figures 3d and 3e show the crystallites in the samples with x=0.21 and 0.31. For these cases the particles are small (generally between 20 and 30 nm), defective and without a definite geometric shape. In the case of sample with x=0.4, remarkable changes occur. The dispersion in crystallites dimension is very large, from several nanometers to 100 nm. At the same time, the EDX measurements evidence large compositional variations through the specimen. Figures 4 (a, b) show the TEM image and the corresponding SAED pattern. Two crystallite morphologies are clearly observed. The large crystallites have a hematite structure and the small ones exhibit the typical cassiterite structure, showing that this sample crystallized as a mixture of the two compounds. The SnO_2 diffraction rings (Figure 4b) reveal a contraction of about 3% of the cassiterite lattice parameters. For x>0.56 the crystallites are small (less than 10 nm) and the samples are quite uniform. The high magnification TEM image in Figure 3g (for x=0.86) is representative of these samples. The uniformity of the crystallites in these two samples is evidenced by the low magnification image in Figure 3h (at x=1.0). For all these samples, the electron diffraction patterns indicate a tetragonal SnO_2 (cassiterite) structure.

Rietveld structure refinements [14] have been performed for the samples at low tin concentrations in order to obtain information concerning the site occupancy in the α-Fe_2O_3 lattice. In the hematite structure the Fe^{3+} ions with coordinates of (0, 0, z) occupy 2/3 of the octahedral holes in successive oxygen layers, and 1/3 of the octahedral holes with coordinates of (0, 0, 0) are empty. In the case of our samples, the best fit was obtained by allowing the presence

of tin ions in both substitutional (0, 0, z) and interstitial (0, 0, 0) sites in the hematite corundum type structure. This finding is in good agreement with the model proposed in reference [11]. The final set of refined parameters are shown in Table 1 and the experimental XRD and calculated profiles are displayed in Figures 5(a, d). It is reasonable that the substitutional and interstitial sites have equal site occupancy. The tin concentrations resulting from the XRD refinement are slightly greater than those measured by EDX.

The refinement of XRD spectra at low tin concentration indicates an increase of the lattice parameters *c* and *a* of the α-Fe_2O_3 structure (Figure 6). This result supports our expectation, because the six coordinated ionic radius of Sn^{4+} is greater (~0.83 Å) than the ionic radius of Fe^{3+} ion (~0.79 Å). The saturation effect observed in Figure 6 starting with x~0.2 suggests the extent of the solubility of Sn^{4+} in the α-Fe_2O_3 lattice. At x~0.7 the rutile phase structure becomes dominant. The lattice parameters *c* and *a,* of the tetragonal SnO_2 cell contract as the content of Fe^{3+} ions increases (Figures 7a, b) suggesting the dissolution of iron ions into SnO_2. The contraction of the SnO_2 lattice parameters, Figure 7, is as much as 3%, in good agreement with electron diffraction data. At x=1.0 the lattice parameters are close to the theoretical values for tetragonal SnO_2.

Figure 8 shows representative ^{57}Fe Mössbauer spectra recorded at room temperature for the hydrothermally synthesized (1-x)α-Fe_2O_3-xSnO_2 nanoparticles. Major changes in Mössbauer line shape and the disappearance of magnetic hyperfine structure as tin content in the samples increases are apparent. The six line pattern at x=0.0 in Figure 8, with hyperfine magnetic field H_{hf}~51.3 T, quadrupole splitting ΔE_Q of -0.29 mm/s and isomer shift δ~0.31 mm/s, is characteristic of the Mössbauer spectrum of the hematite structure [15]. The continuous line represents the fit of the hypothesized Lorentzian lineshape. The presence of Sn^{4+} ions in the system increases the complexity of the computer fit. For the fit, we have to consider the

preference of tin ions for octahedral positions as well as that the hyperfine field corresponds to different environments at the iron nucleus. In our system at least three different nearest-neighbor interactions could exist: iron–iron, iron-tin and iron-cation vacancy. These possible interactions imply that at least three magnetic sublattices have to be considered in the computer fit. The fit obtained with this approximation was far from acceptable. The best fit was obtained by using a distribution of hyperfine fields. Representative Mössbauer spectra and the corresponding sublattices are presented in Figure 9 (a, b, c), together with the magnetic hyperfine field distribution probabilities given by the computer fit (Figure 9 A, B, C) for the samples with x=0.08, x=0.21 and x=0.31. At x=0.08 the distribution is rather narrow and can be well approximated with a Lognormal one; this behavior reflects minor changes in the electron spin density at the iron nucleus due to small amounts of tin neighboring ions. The Mössbauer spectra at x=0.21 and 0.31 as well as the resulting magnetic hyperfine distributions (Figure 9 B, C) reflect the spectacular changes in the structure as the tin content increases. The best fit with the data has been obtained considering a hyperfine magnetic field distribution accompanied by a central quadrupole doublet. The distribution is spread out to lower values and presents some small peaks reflecting a high degree of disorder in the structure. The maximum values of magnetic hyperfine fields remain close to the hematite value but the probability drops with the increase of Sn^{4+} in the system. The maximum hyperfine field value in the distribution can be ascribed to Fe^{3+} ions without Sn^{4+} in nearby lattice sites, while the distributions at lower magnetic fields reflects the lower spin density at Fe^{3+} in the vicinity of Sn^{4+} nearest neighbors. This behavior suggests that we are not dealing with relaxation effects due to the dilution of a magnetic system (or superparamagnetic effects associated with the decreasing of particle dimension) but with the diminishing of hematite-like phase as the tin content in samples increases. The intensity of the central quadrupole doublet increases as the magnetic component

in the system decreases and becomes the dominant pattern in the Mössbauer spectra at greater tin concentration (Figure 8). The related Mössbauer hyperfine parameters of the order of 0.77 mm/s for ΔE_Q and 0.38 mm/s for δ, and line width close to the natural one, approximately constant from x=0.21 till x=0.86, are appropriate for Fe^{3+} in the 'S' state. Taking into account the appearance of the broadened rutile type structure in the XRD spectra at x≥0.21 (Figures 1c, 1d) we can assign the doublet in the Mössbauer spectrum to Fe^{3+} ions substituting for Sn^{4+} in the tetragonal SnO_2 structure. It is known [16] that 3-d transition element impurities enter the lattice substitutionally at Sn^{4+} site and specifically that iron enters the lattice in its high spin ferric state $^6S_{5/2}$. In SnO_2 each tin ion is octahedrally surrounded by six oxygen ions at nearly equal distances. If an iron ion substitutes for a tin ion, an axial distortion is formed because of the different ionic radii and different ionic charge. This distortion is seen in the Mössbauer spectra in a quadrupole splitting of given amplitude. Considering the behavior of XRD spectra, as well as the TEM and EDX data, the evolution of the central quadrupole doublet versus tin content in these samples is an argument for the crystallization of a SnO_2-like structure in the hydrotermally synthesized $(1-x)\alpha\text{-}Fe_2O_3\text{-}xSnO_2$ nanoparticles.

The comparison of magnetic versus paramagnetic phase (quadrupole doublet) in the nanoparticles system $(1-x)\alpha\text{-}Fe_2O_3\text{-}xSnO_2$, as determined from Mössbauer spectra, is represented in Figure 10. From this graph we can infer that the solubility of SnO_2 in $\alpha\text{-}Fe_2O_3$ is limited to x~0.2 in the nanoparticle system $(1-x)\alpha\text{-}Fe_2O_3\text{-}xSnO_2$ synthesized under hydrothermal conditions which is in good agreement with our XRD results. This value represents an unexpectedly high solublitiy of SnO_2 in $\alpha\text{-}Fe_2O_3$ in comparison with the thermodynamic equilibrium state of only 1 mole % or less at 1073 K [9]. From our XRD and Mössbauer data, the substitution of iron in the SnO_2 lattice, crystallized under hydrothermal conditions, is clearly possible for x≥0.7, although the cassiterite phase containing iron is present as early as at x≥0.21. These findings

agree with the solubility estimated in the reference [10], where the α-Fe_2O_3-SnO_2 fine particle system was prepared by thermal decomposition at 873 K, in the presence of a few percent of $(SO_4)^{2-}$. Figures 11 and 12 show the particle morphology and stoichiometry determined by SEM and EDX examinations of the hematite-tin oxide system for x=0.4. Our XRD, Mössbauer spectroscopy, TEM and EDX investigations are consistent with a solubility of SnO_2 and α-Fe_2O_3 in each other over a wide composition range.

Table 1. Ion positions, site occupancy, reliability R factors and lattice parameters obtained in the Rietveld structure refinement of XRD patterns for (1-x)α-Fe_2O_3-xSnO_2 nanoparticles, at x = 0.0, 0.08, 0.15 and 0.21.

Sample (x)	***Atom***	***x/a***	***y/b***	***z/c***	***Site occupancy***	***Reliability R factors (%)***	***Lattice parameters (Å)***
x = 0.0	Fe	0.0	0.0	0.3553	1.0	Rp = 7.84 Rwp = 10.98 Rexp = 6.63	*a* = 5.0341 *c* = 13.7482
	O	0.3059	0.0	0.25	1.0		
x = 0.08	Fe	0.0	0.0	0.3547	0.930	Rp = 7.57 Rwp = 10.11 Rexp = 6.77	*a* = 5.0509 *c* = 13.7871
	Sn1	0.0	0.0	0.3547	0.035		
	Sn2	0.0	0.0	0.0	0.035		
	O	0.3079	0.0	0.25	1.0		
x = 0.15	Fe	0.0	0.0	0.3549	0.870	Rp = 9.91 Rwp =12.56 Rexp = 5.01	*a* = 5.0592 *c* = 13.7983
	Sn1	0.0	0.0	0.3549	0.065		
	Sn2	0.0	0.0	0.0	0.065		
	O	0.3081	0.0	0.25	1.0		
x = 0.21	Fe	0.0	0.0	0.3510	0.810	Rp = 11.57 Rwp = 15.62 Rexp = 3.14	*a* = 5.0693 *c* = 13.8093
	Sn1	0.0	0.0	0.3510	0.095		
	Sn2	0.0	0.0	0.0	0.095		
	O	0.3084	0.0	0.25	1.0		

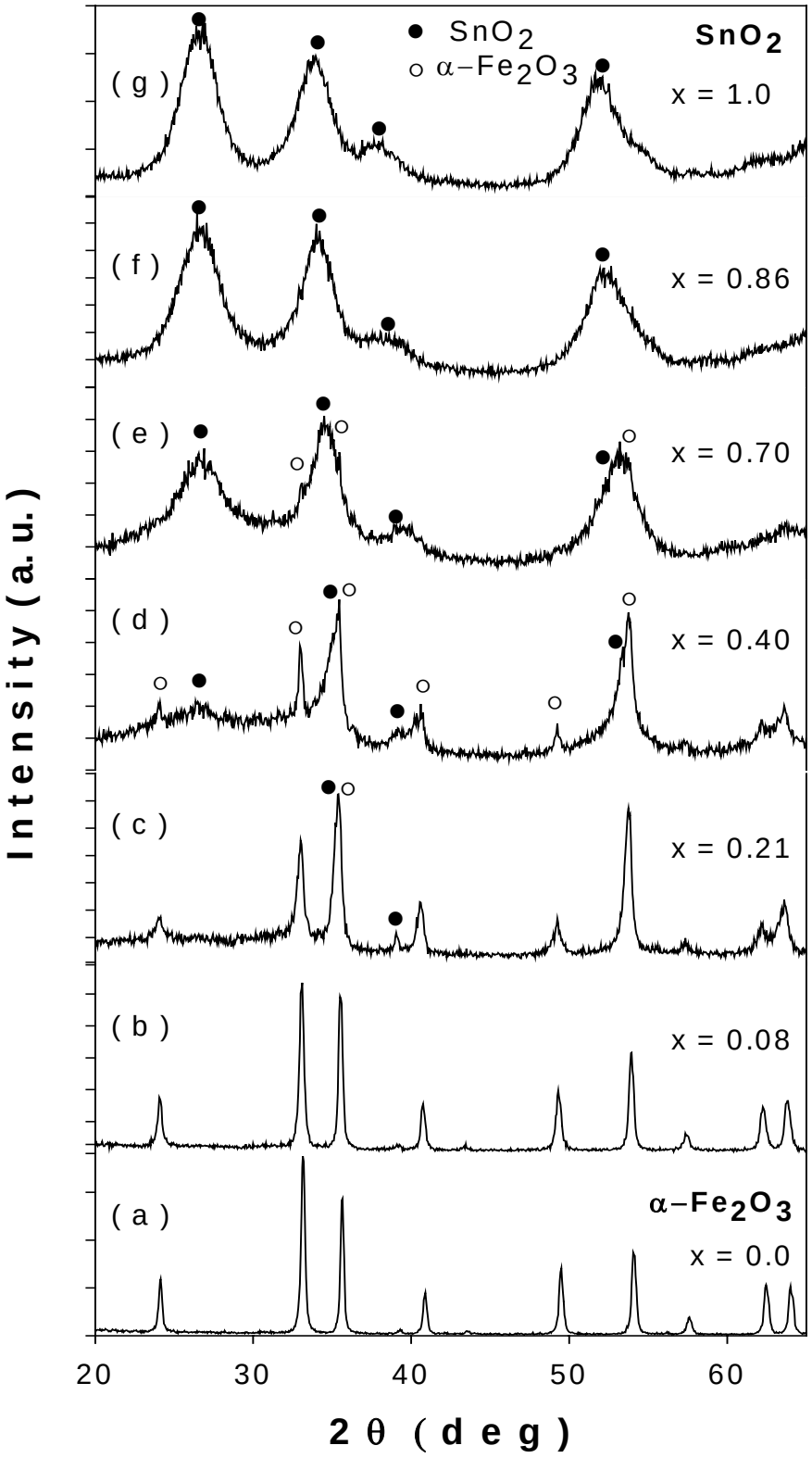
● SnO2
○ α–Fe2O3
SnO2
x = 1.0
(g)
(f)
x = 0.86
(e)
x = 0.70
(d)
x = 0.40
(c)
x = 0.21
(b)
x = 0.08
(a)
α–Fe2O3
x = 0.0
Intensity (a.u.)
20
30
40
50
60
2θ (deg)

Figure 1

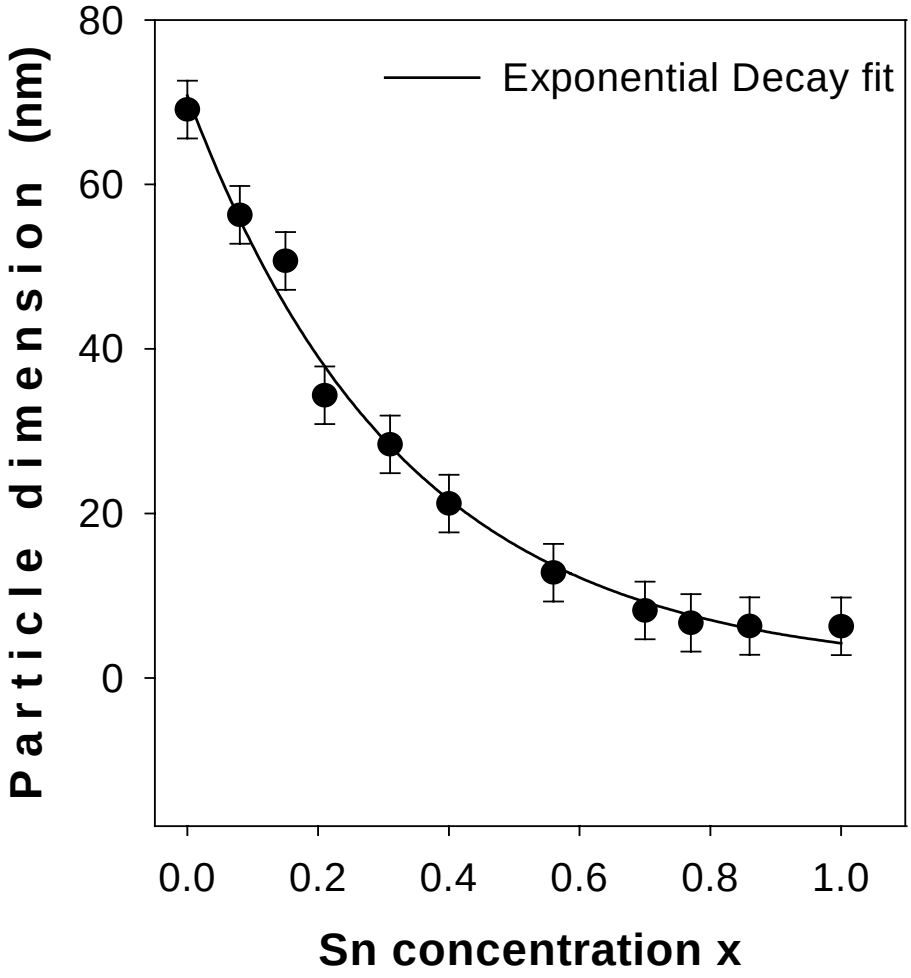
Exponential Decay fit
Particle dimension (nm)
80
60
40
20
0
0.0
0.2
0.4
0.6
0.8
1.0
Sn concentration x

Figure 2

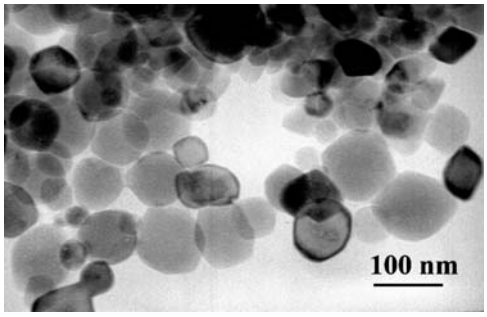

(a) x = 0.0

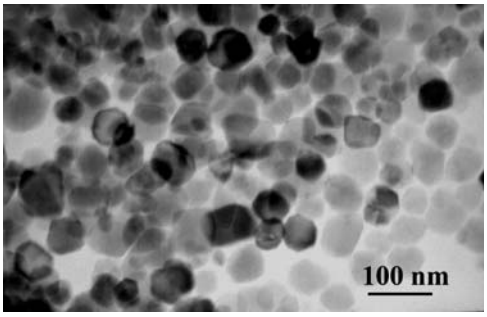

(b) x = 0.08

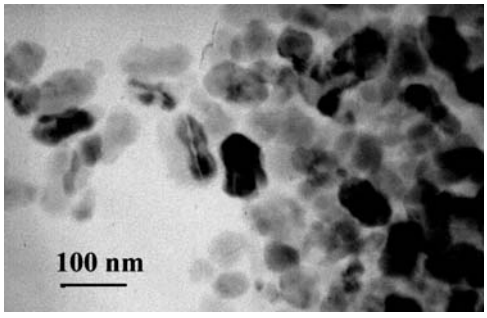

(c) x = 0.15

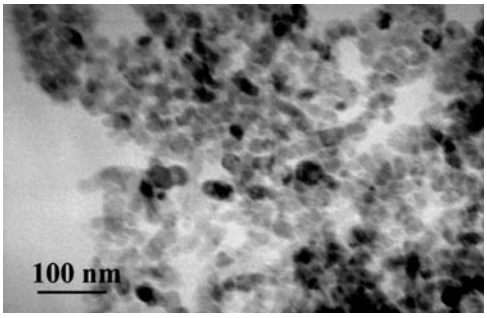

(d) x = 0.21

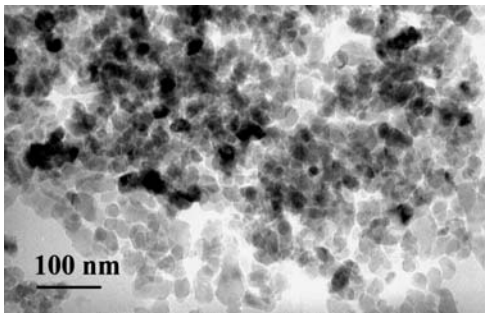

(e) x = 0.31

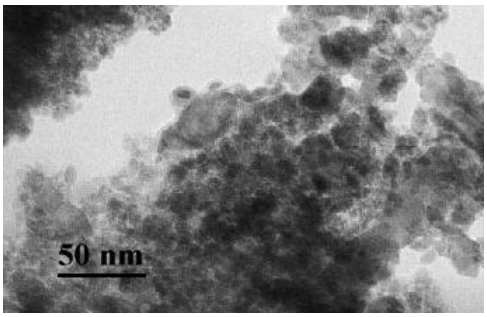

(f) x = 0.4

(g) x = 0.86

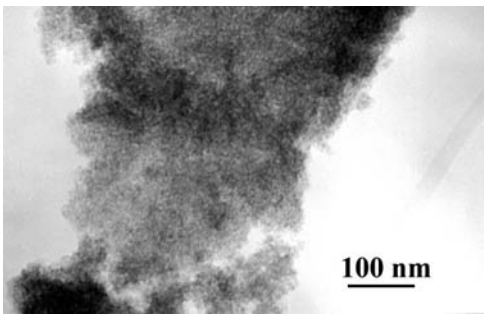

(h) x = 1.0

Figure 3

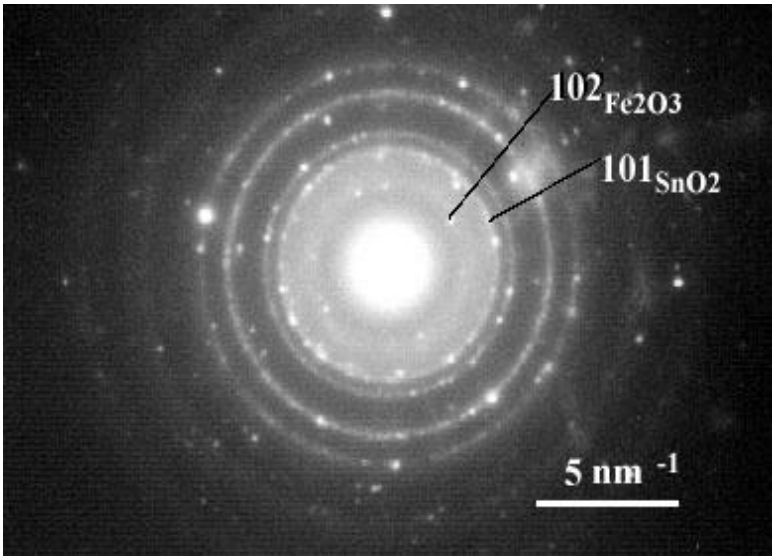

(b)

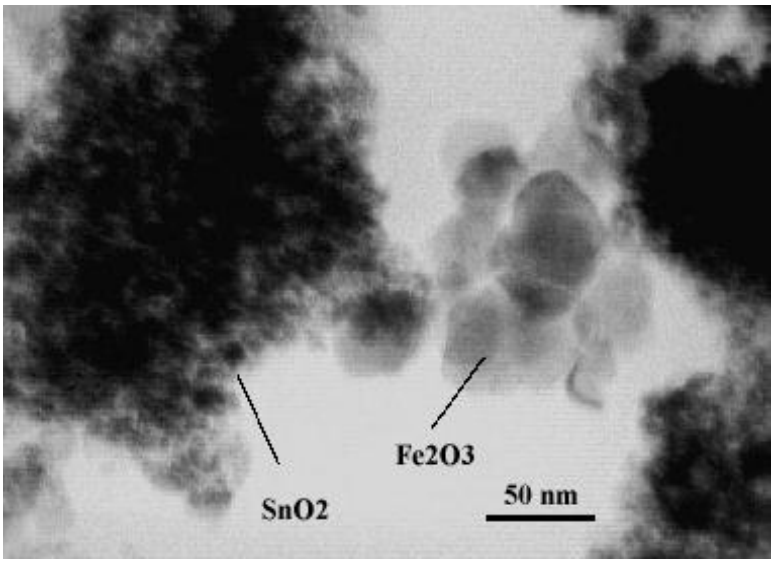

(a)

Figure 4

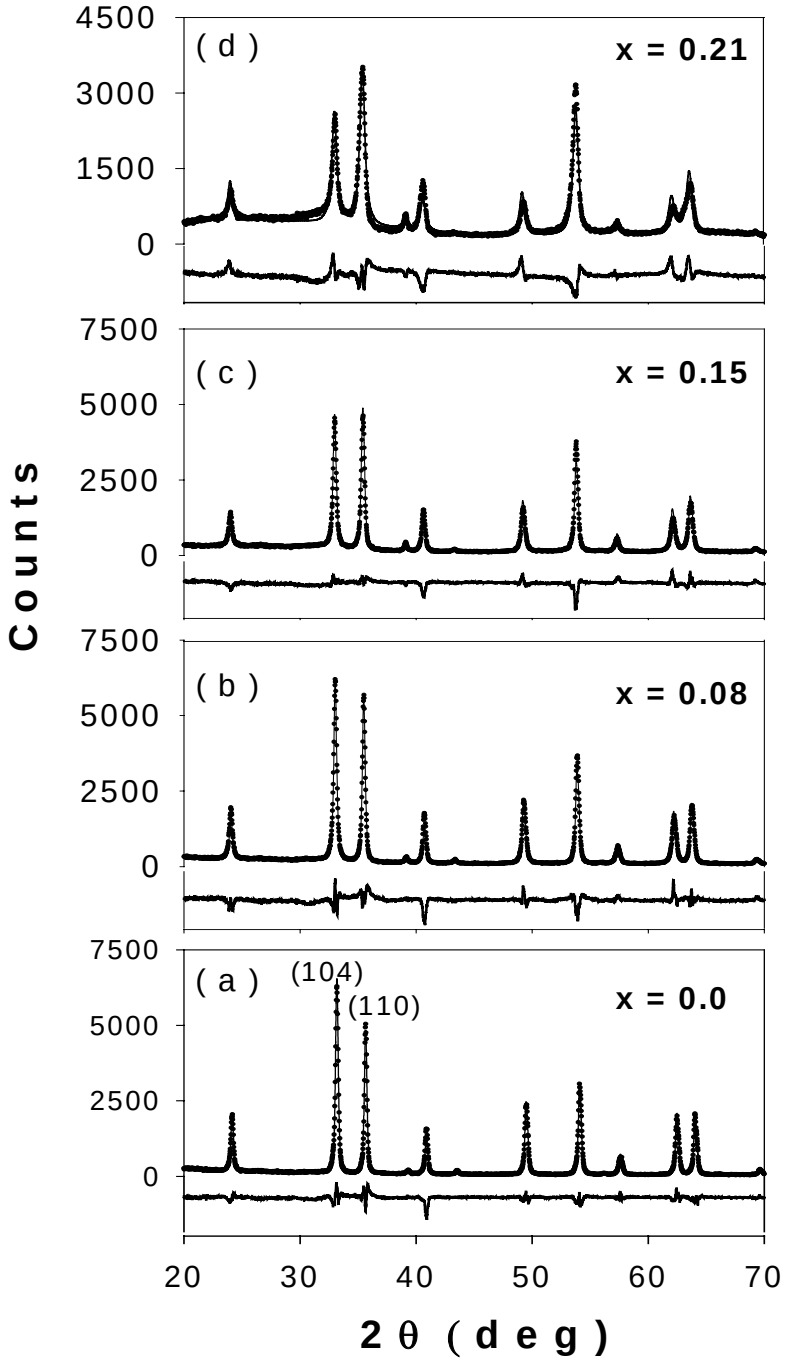
4500
3000
1500
0
(d)
x = 0.21
7500
5000
2500
0
(c)
x = 0.15
7500
5000
2500
0
(b)
x = 0.08
7500
5000
2500
0
(a)
(104)
(110)
x = 0.0
Counts
20
30
40
50
60
70
2 θ (d e g)

Figure 5

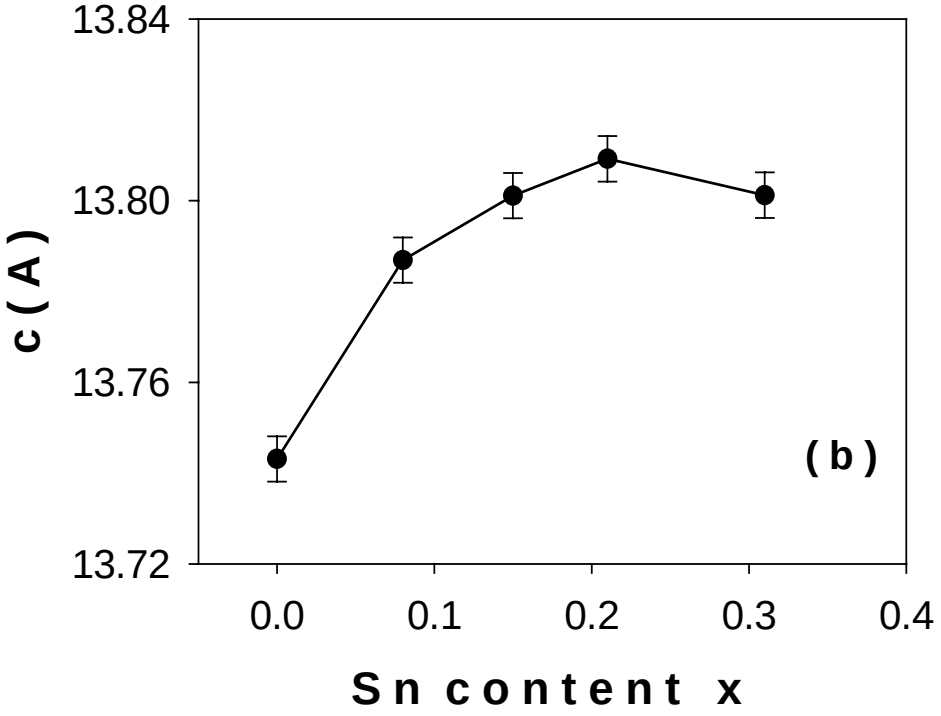
13.84
13.80
13.76
13.72
c (A)
(b)
0.0
0.1
0.2
0.3
0.4
Sn content x

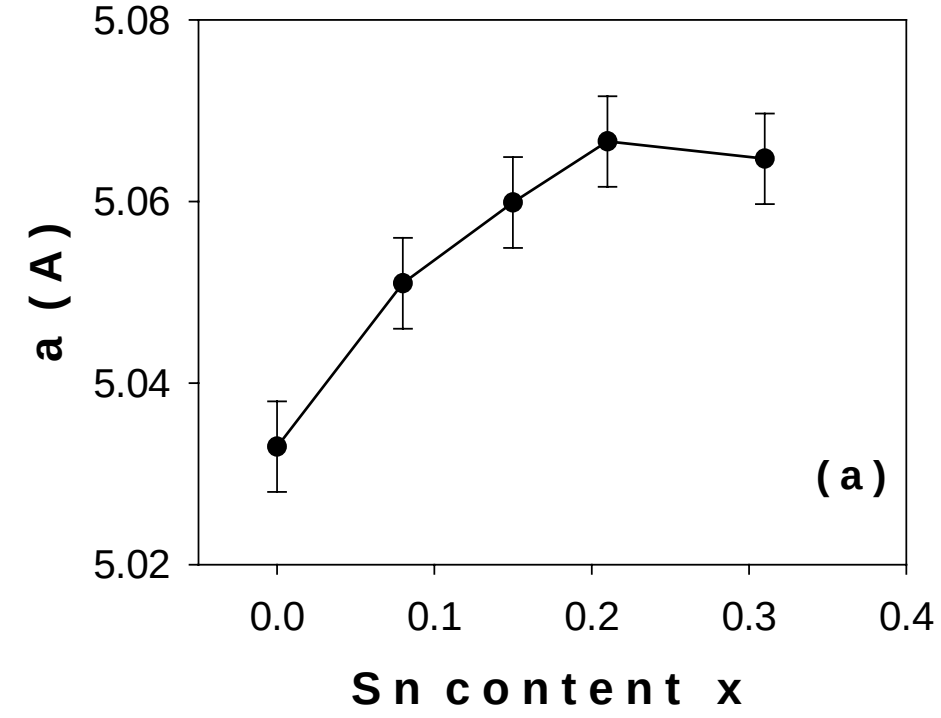
5.08
5.06
5.04
5.02
a (A)
(a)
0.0
0.1
0.2
0.3
0.4
Sn content x

Figure 6

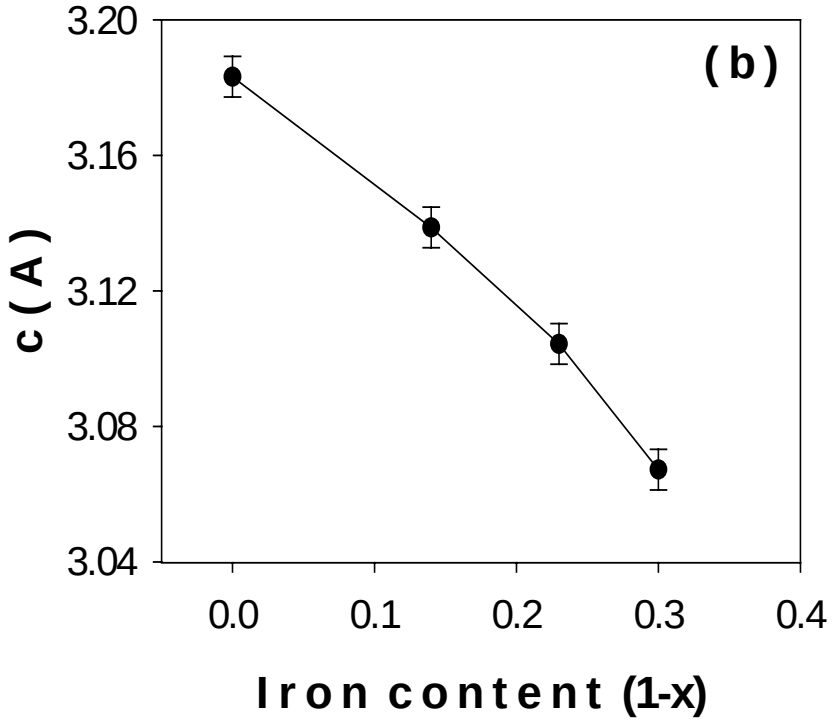
(b)
3.20
3.16
3.12
3.08
3.04
c (A)
0.0
0.1
0.2
0.3
0.4
Iron content (1-x)

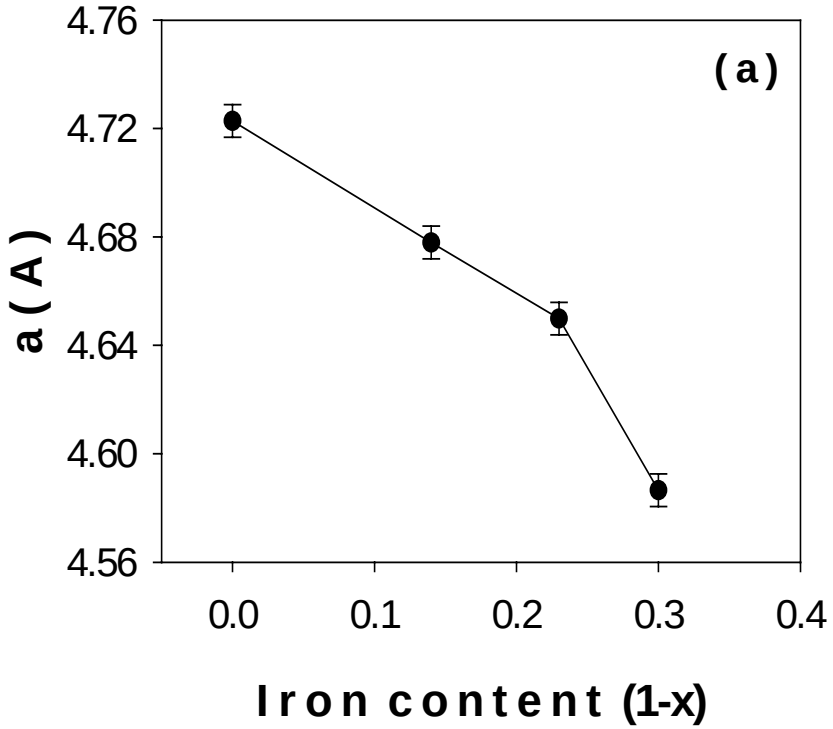
(a)
4.76
4.72
4.68
4.64
4.60
4.56
a (A)
0.0
0.1
0.2
0.3
0.4
Iron content (1-x)

Figure 7

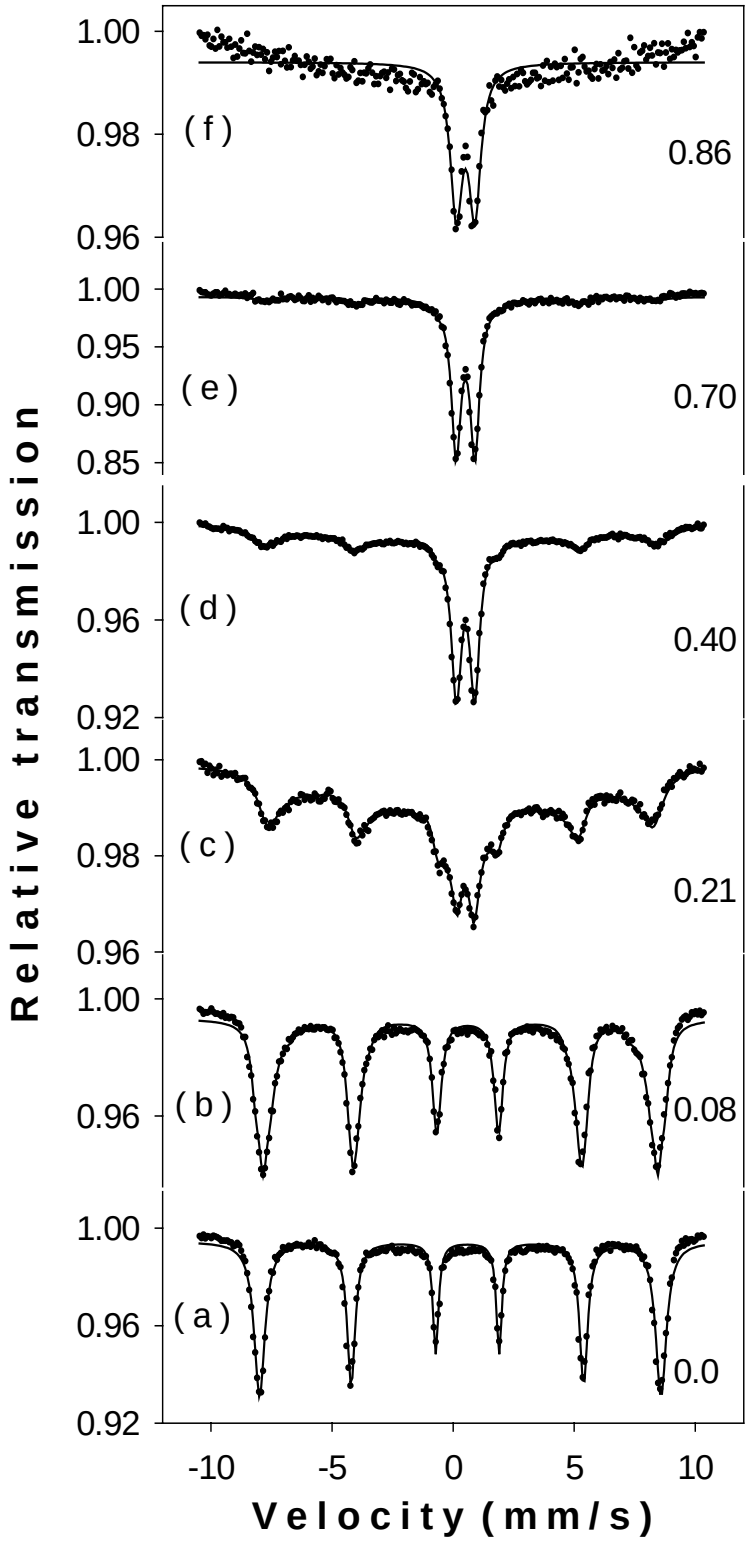
Relative transmission
1.00
0.98
0.96
(f)
0.86
1.00
0.95
0.90
0.85
(e)
0.70
1.00
0.96
0.92
(d)
0.40
1.00
0.98
0.96
(c)
0.21
1.00
0.96
(b)
0.08
1.00
0.96
0.92
(a)
0.0
-10
-5
0
5
10
Velocity (mm/s)

Figure 8

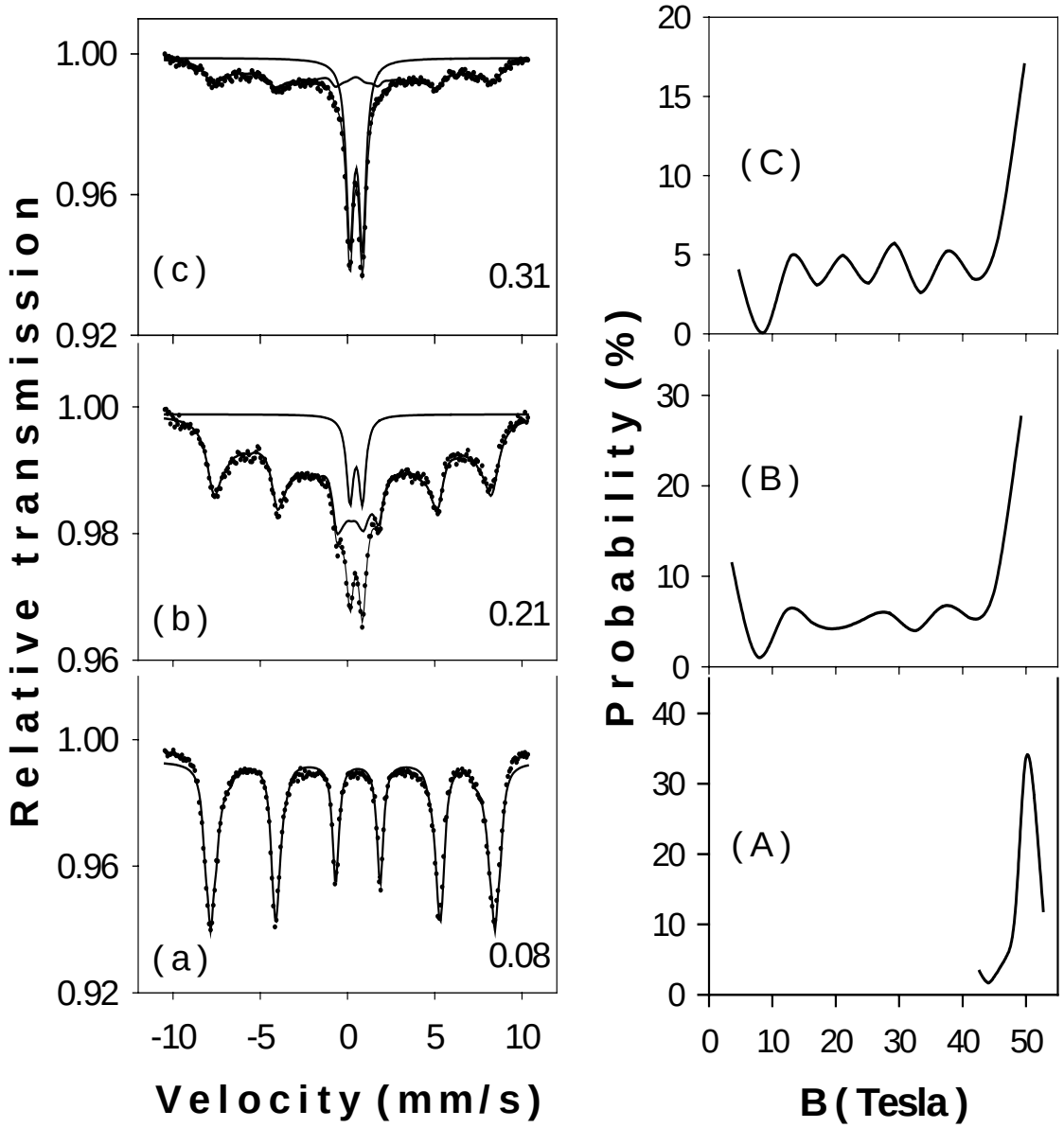
Relative transmission
1.00
0.96
0.92
(c)
0.31
1.00
0.98
0.96
(b)
0.21
1.00
0.96
0.92
(a)
0.08
-10
-5
0
5
10
Velocity (mm/s)
Probability (%)
20
15
10
5
0
(C)
30
20
10
0
(B)
40
30
20
10
0
(A)
0
10
20
30
40
50
B (Tesla)

Figure 9

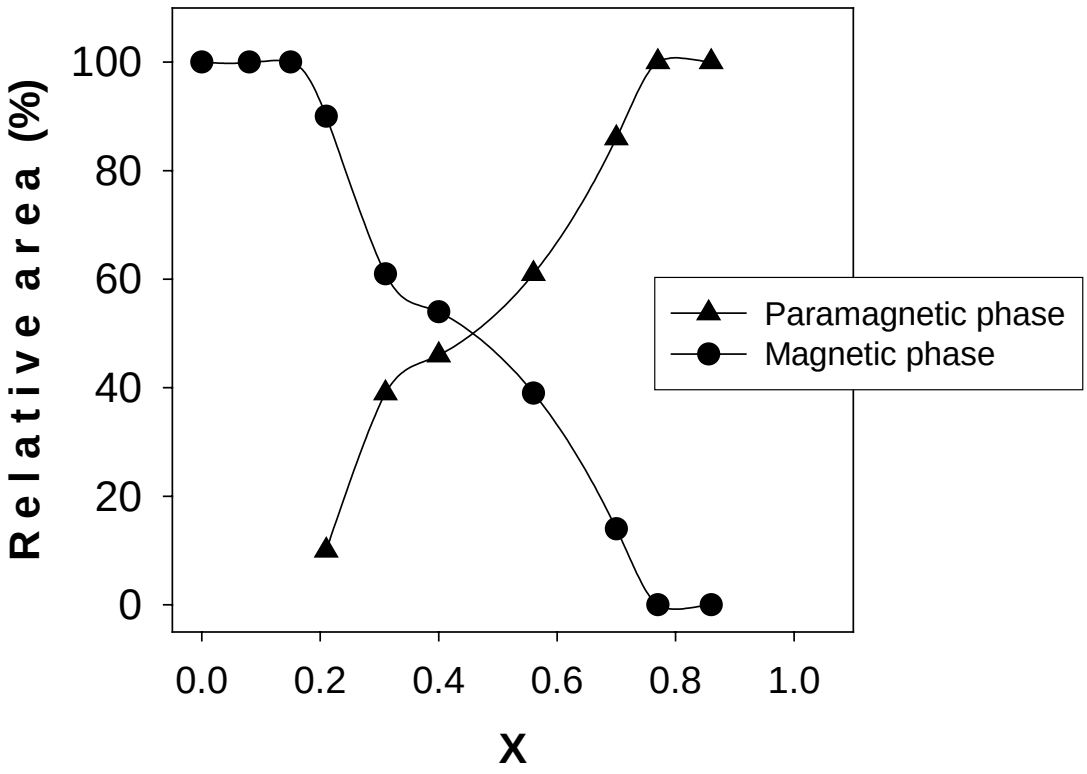
Relative area (%)
100
80
60
40
20
0
0.0
0.2
0.4
0.6
0.8
1.0
X
Paramagnetic phase
Magnetic phase

Figure 10

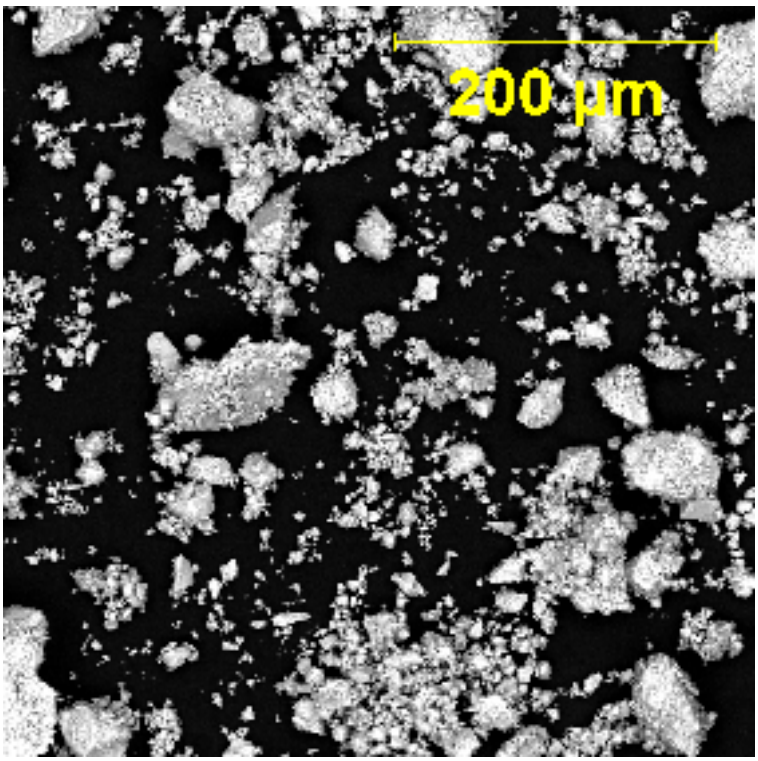

Figure 11

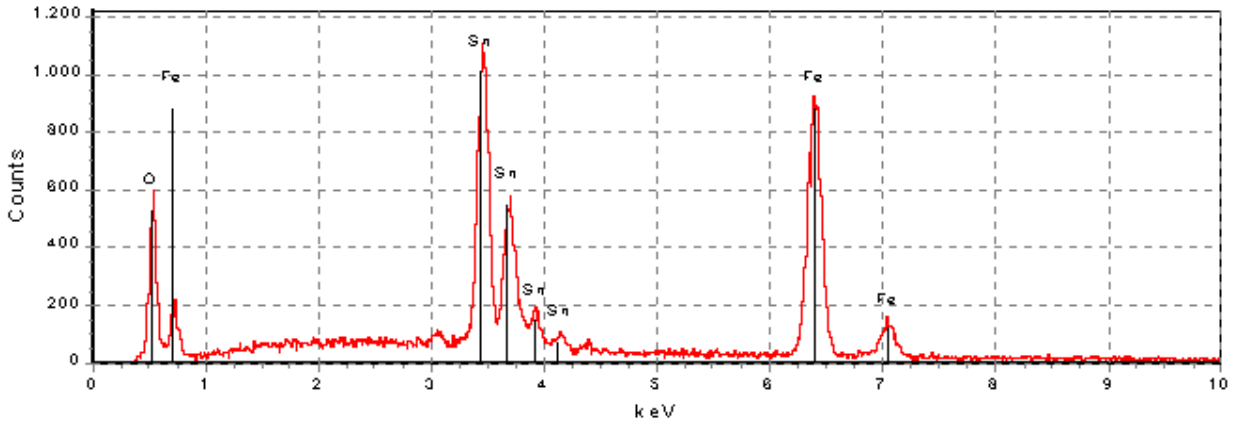

Figure 12

CONCLUSIONS

The (1-x)α-Fe_2O_3-xSnO_2 nanoparticles system has been obtained through a hydrothermal route under relatively mild conditions of temperature and pressure (200 ˚C and p~15 atm). The mean particle diameter decreases from 70 to 6 nm as tin molar concentration increases up to x=1.0. The Rietveld structure refinements of the XRD spectra at low tin concentrations are consistent with the presence of Sn^{4+} in α-Fe_2O_3 structure in two different sites: substituting for Fe^{3+} in octahedral sites (0, 0, z) and occupying some interstitial sites (0,0,0) normally vacant in the hematite structure. At greater Sn concentrations, a tetragonal SnO_2 structure crystallizes, where the Fe^{3+} ions partially substitute for Sn^{4+} ions in the structure. The estimated solubility limits in the nanoparticle system (1-x)α-Fe_2O_3-xSnO_2 synthesized under the hydrothermal conditions are: $x \leq 0.2$ for Sn^{4+} in the α-Fe_2O_3 and $x \geq 0.7$ for Fe^{3+} in SnO_2. This paper is the first report on the hydrothermal synthesis and structural characterization of (1-x)α-Fe_2O_3-xSnO_2 system over the full range of tin concentration, from x=0.0 to x=1.0. Moreover, this synthesis route allowed us to reach the nanometric particle dimensions, which would make them very attractive for sensing applications.

REFERENCES

[1] Gopel W., *Sens. Actuators* **B 18-19**, 1 (1994).

[2] Yamazoe N. and Miura N., *Sens. Actuators* **B 20**, 95 (1994).

[3] Tamaki J., Naruo C., Yamamoto Y. and Matsuoka M., *Sens. Actuators* **B 83**, 190 (2002).

[4] Jiang J.Z., Liu R., Morup S., Nielsen K., Poulsen F.W., Berry F.J. and Clasen R., *Phys. Rev.* **B 55**, 11 (1997).

[5] Jiang J.Z., Liu R., Nielsen K., Morup S., Dam-Johansen K. and Clasen R., *J. Phys. D*: *Appl. Phys*. **30**, 1459 (1997).

[6] Zhu W., Tan O.K. and Jiang J.Z., *J. Mater. Sci: Mater. Electron* **9**, 275 (1998).

[7] Tan O.K., Zhu W., Yan Q. and Kong L.B., *Sens. Actuators* **B 65,** 361 (2000).

[8] Gopal Reddy C.V., Cao W., Tan O.K. and Zhu W., *Sens. Actuators* **B 81**, 170 (2002).

[9] Cassedanne J., *An. Acad. Bras. Cienc*. **38**, 265 (1966).

[10] Takano H., Bando Y., Nakanishi N., Sakai M. and Okinaka H., *J. Sol. St. Chem*. **68**, 153 (1987).

[11] Berry F.J., Greaves C., McManus J.G., Mortimer M. and Oates G., *J. Sol. St. Chem*. **130**, 272 (1997).

[12] Berry F.J., Bohorquez A., Helgason O, Jiang J.Z., McManus J.G., Moore E., Mortimer M., Mosselmans F. and Morup S., *J. Phys. Cond. Matter*. **12**, 4043 (2000).

[13] Klug H.P. and Alexander L.E., X-*ray diffraction procedures for polycrystalline and amorphous materials*, (J. Wiley and Sons, New York, 1966**)** p. 491.

[14] The Rietveld Method, edited by R.A. Young (Oxford University Press, New York, 1993).

[15] Greenwood N.N., Gibb T.C., *Mössbauer spectroscopy*, (Chapman and Hall Ltd., London 1971) p. 241.

[16] Nakada R., Ebina A. and Takahashi T., *J. Phys. Soc. Japan* **21**, 188 (1966).

LIST OF ACRONYMS AND ABBREVIATIONS

XRD=X-ray diffraction

SEM=Scanning electron microscopy

TEM=Transmission electron microscopy

EDX=Energy dispersive X-ray analysis

LIST OF PUBLICATIONS

M. Sorescu, L. Diamandescu, D. Tarabasanu-Mihaila, V.S. Teodorescu and B.H. Howard, "Hydrothermal Synthesis and Structural Characterization of $(1-x)\alpha$-Fe_2O_3-$xSnO_2$ Nanoparticles", **Journal of Physics and Chemistry of Solids**, in press.

Since the last report the following papers were published or accepted for publication:

1) **M. Sorescu**, F. Pourarian and R.A. Brand, "Mössbauer Study of Hydrogenation Effects in Iron-Rich Intermetallics", **Journal of Materials Science Letters** 22 (2003) 1569-1572.

2) **M. Sorescu**, A. Grabias, L. Diamandescu and D. Tarabasanu-Mihaila, "Bulk Versus Surface Effects in Magnetic Thin Films Obtained by Pulsed Laser Deposition", **Applied Surface Science**, 217 (2003) 233-238.

3) **M. Sorescu** and M. Valeanu, "Effect of Substitutions on the Hyperfine Magnetic Field in Nd-Based Intermetallics", **Intermetallics** 11 (2003) 749-754.

4) **M. Sorescu**, F. Pourarian and R.A. Brand, "Mossbauer Study of Hydrogenation Effects in Iron-Rich Intermetallics", **Journal of Materials Science Letters** 22 (2003) 1569-1572.

5) **M. Sorescu**, A. Grabias and M. Valeanu, "A Mössbauer Study of Spring Magnets", **IEEE Transaction on Magnetics** 39 (2003) 2959-2961.

6) **M. Sorescu**, L. Diamandescu and A. Grabias, "Evolution of Phases During Mechanochemical Activation in Magnetite-Containing Systems", **Materials Chemistry and Physics** 83 (2004) 354-360.

7) **M. Sorescu**, L. Diamandescu, D. Tarabasanu-Mihaila and V.S. Teodorescu, "Nanocrystalline Rhombohedral In_2O_3 Synthesized by Hydrothermal and Postannealing Pathways", **Journal of Materials Science** 39 (2004) 675-677.

8) **M. Sorescu**, L. Diamandescu, R. Peelamedu, R. Roy and P. Yadoji, "Structural and Magnetic Properties of NiZn Ferrites Prepared by Microwave Sintering", **Journal of Magnetism and Magnetic Materials**, in press.

9) **M. Sorescu**, L. Diamandescu, R.A. Brand and D. Tarabasanu-Mihaila, "Mössbauer Study of Manganese-Doped Magnetite Below the Verwey Transition", **Materials Letters** 58 (2004) 885-888.